Compartmentalization of androgen receptor protein–protein interactions in living cells

Martin E. van Royen,[1] Sónia M. Cunha,[1] Maartje C. Brink,[2] Karin A. Mattern,[1] Alex L. Nigg,[1] Hendrikus J. Dubbink,[1] Pernette J. Verschure,[2] Jan Trapman,[1] and Adriaan B. Houtsmuller[1]

[1]Department of Pathology, Josephine Nefkens Institute, Erasmus MC, 3000 CA Rotterdam, Netherlands
[2]Structure and Functional Organisation of the Cell Nucleus, Swammerdam Institute for Life Sciences, University of Amsterdam, 1090 GB Amsterdam, Netherlands

Steroid receptors regulate gene expression in a ligand-dependent manner by binding specific DNA sequences. Ligand binding also changes the conformation of the ligand binding domain (LBD), allowing interaction with coregulators via LxxLL motifs. Androgen receptors (ARs) preferentially interact with coregulators containing LxxLL-related FxxLF motifs. The AR is regulated at an extra level by interaction of an FQNLF motif in the N-terminal domain with the C-terminal LBD (N/C interaction). Although it is generally recognized that AR coregulator and N/C interactions are essential for transcription regulation, their spatiotemporal organization is largely unknown. We performed simultaneous fluorescence resonance energy transfer and fluorescence redistribution after photobleaching measurements in living cells expressing ARs double tagged with yellow and cyan fluorescent proteins. We provide evidence that AR N/C interactions occur predominantly when ARs are mobile, possibly to prevent unfavorable or untimely cofactor interactions. N/C interactions are largely lost when AR transiently binds to DNA, predominantly in foci partly overlapping transcription sites. AR coregulator interactions occur preferentially when ARs are bound to DNA.

Introduction

The androgen receptor (AR) is a ligand-dependent transcription factor of the steroid receptor (SR) subfamily of nuclear receptors. ARs regulate expression of genes involved in development and maintenance of the male phenotype and play a role in the growth of prostate cancer. Like all SRs, AR is composed of a central DNA binding domain (DBD), a C-terminal ligand binding domain (LBD), and an N-terminal transactivation domain (NTD; Brinkmann et al., 1989). In the absence of androgens, ARs are mainly located in the cytoplasm. Upon ligand binding, ARs rapidly translocate to the nucleus, where they bind to androgen response elements (AREs) in the promoters/enhancers of target genes and recruit transcriptional coregulators (Cleutjens et al., 1997; Claessens et al., 2001; Rosenfeld et al., 2006). Many coregulators, like the p160 family, bind via LxxLL motifs to a hydrophobic cleft in the LBD of SRs formed by ligand-induced repositioning of the C-terminal α-helix. The AR differs from the other SRs in that its LBD preferentially interacts with cofactors containing FxxLF rather than LxxLL motifs (Dubbink et al., 2004; Hur et al., 2004). In addition, an extra level of regulation of AR function is provided by an FQNLF motif in its NTD, which is able to interact with the liganded C-terminal LBD (N/C interaction; Doesburg et al., 1997; He et al., 2000). A well-recognized function of N/C interaction is stabilization of ligand binding (He et al., 2001; Dubbink et al., 2004). In addition, it has been hypothesized that N/C interactions might block unfavorable protein–protein interactions.

Confocal microscopy of GFP-tagged proteins, as well as quantitative assays such as FRAP and fluorescence resonance energy transfer (FRET), have been instrumental in the investigation of the behavior of SRs in living cells (Georget et al., 1997; McNally et al., 2000; Stenoien et al., 2001; Schaaf and Cidlowski, 2003; Farla et al., 2004, 2005; Michalides et al., 2004; Agresti et al., 2005; Rayasam et al., 2005; Schaufele et al., 2005). Like many other nuclear factors interacting with DNA, SRs, including the AR, were shown to be highly mobile in the living cell nucleus and dynamically interact with specific binding sites (McNally et al., 2000; Stenoien et al., 2001; Farla et al., 2004, 2005; Rayasam et al., 2005; Marcelli et al., 2006). We have previously shown, using FRAP analysis based on computer modeling, that agonist-bound ARs are largely mobile in the nucleus and only

Correspondence to A.B. Houtsmuller: a.houtsmuller@erasmusmc.nl

Abbreviations used in this paper: AR, androgen receptor; ARE, androgen response element; BrUTP, 5-bromo-uridine-5′-triphosphate; DBD, DNA binding domain; FRET, fluorescence resonance energy transfer; LBD, ligand binding domain; NTD, N-terminal transactivation domain; SR, steroid receptor.

The online version of this article contains supplemental material.

The Journal of Cell Biology, Vol. 177, No. 1, April 9, 2007 63–72
http://www.jcb.org/cgi/doi/10.1083/jcb.200609178

transiently bind to immobile elements in the nucleus. This transient immobilization was most likely due to DNA binding, as several non–DNA binding mutants were freely mobile and did not show a detectable immobile fraction (Farla et al., 2004, 2005). In addition, a recent elegant study using ARs double tagged at the N and C termini with the FRET couple CFP and YFP, respectively, has revealed that N/C interactions are initiated promptly after the addition of hormone, before transport to the nucleus (Schaufele et al., 2005). However, questions regarding the spatiotemporal organization of AR in the nuclei of live cells remain unanswered: when, where, and in what order do interactions with coregulators and N/C interaction take place once an AR has entered the nucleus? Does proper regulation of AR function require compartmentalization of such interactions? In this study, we applied innovative combined FRAP and FRET methodology, and ratio imaging, using CFP and YFP tagging of wild-type ARs and AR mutants, to investigate the spatiotemporal regulation of AR N/C interactions and AR coregulator interactions in living cells.

Results

ARs double tagged with CFP and YFP are functional

We tagged the fluorescent proteins YFP and CFP to the N and C termini of wild-type AR (YFP-AR-CFP) and to two mutant ARs: an N/C interaction–deficient mutant in which the N-terminal FQNLF motif is changed into an AQNAA motif (AR[F23,27A/L26A]), and the non–DNA binding mutant carrying a point mutation in the DBD, leading to the inability of this mutant to bind to androgen-regulated promoters (AR[A573D]; Fig. 1 A). Western blot analysis showed that the expressed fusion proteins were all of the expected size (Fig. 1 B). In addition, several lines of evidence show that the double tag does not abolish AR function: the wild-type YFP-AR-CFP was able to induce expression of a luciferase reporter gene driven by an androgen-regulated promoter (at ~35% of the activity of the untagged AR), whereas the DBD mutant YFP-AR(A573D)-CFP was not (Fig. 1 C). Importantly, although the transcription activation of double-tagged ARs was lower than that of untagged ARs, the presence of the F23,27A/L26A mutations reduced the activity of both double-tagged and untagged AR to the same extent (~60% reduction), showing that the transcriptional activity of double-tagged ARs is sufficient to investigate its behavior (Fig. 1 C). Furthermore, the fusion proteins were mainly cytoplasmic in the absence of androgens and, after the addition of the agonistic ligand R1881, translocated to the nucleus at normal rate (Georget et al., 1997; unpublished data). In the nucleus, the typical punctate nuclear distribution patterns were observed for the double-tagged wild-type AR and the double-tagged AR(F23,27A/L26A) mutant, whereas the inactive non–DNA binding mutant YFP-AR(A573D)-CFP displayed the typical homogeneous distribution pattern described previously (Fig. 1 D; Farla et al., 2004). In summary, these data show that double tagging the AR and AR mutants did not interfere with their native behavior.

FRET in double-tagged YFP-AR-CFP represents AR N/C interaction

We then investigated whether the double-tagged YFP-AR-CFP provided a bonafide tool to study N/C interaction by FRET.

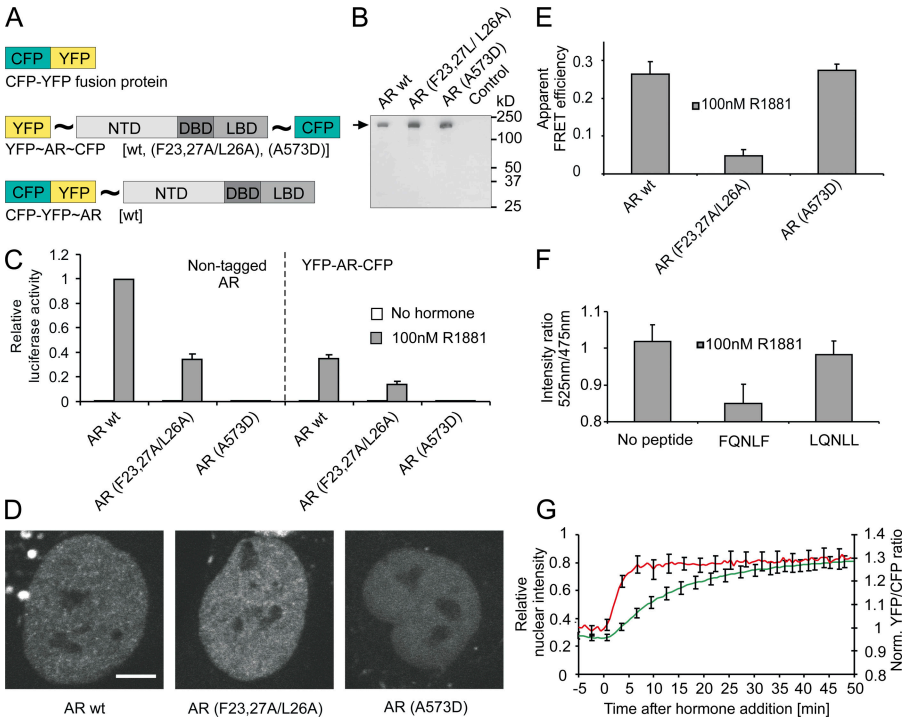

Figure 1. **FRET measured on double YFP- and CFP-tagged AR represent the FQNLF-mediated N/C interaction.** (A–D) Transactivating capacity and nuclear distribution of CFP- and YFP-tagged AR constructs are not affected by the double tags. (A) Schematic representation of the fusion proteins (squiggly line represents a $[Gly\text{-}Ala]_6$ spacer). (B) Western blot of the fusion proteins expressed in Hep3B cells. (C) Transactivation activity of untagged and double-tagged wild-type and mutant ARs as measured on a $(ARE)_2$-TATA Luc reporter. Means ± SEM of five independent experiments are shown. (D) Confocal images of nuclei of Hep3B cells stably expressing the indicated proteins in the presence of R1881. Bar, 5 µm. (E–G) FRET of YFP-AR-CFP represents FQNLF-mediated N/C interaction. (E) Acceptor photobleaching FRET (abFRET; Fig. S2 A, available at http://www.jcb.org/cgi/content/full/jcb.200609178/DC1) of the indicated proteins shows loss of N/C interaction in the AR(F23,27A/L26A) mutant, but not in the A573D mutant. Data shown are the mean ± SEM of at least three independent experiments in which a mean of 15 cells were measured. (F) Spectroscopic analysis of cell lysates of Hep3B cells expressing YFP-AR-CFP shows that FQNLF peptide motifs, but not LQNLL, inhibit interaction. Means ± SEM of three independent experiments are shown. (G) Simultaneous detection of YFP and CFP signals (at 458 nm excitation) shows a prompt increase of YFP/CFP ratio after R1881 addition at t = 0 min (red line; $n = 10$). Translocation to the nucleus (green line) is much slower, indicating that N/C interaction (red line) depends on hormone binding rather than cytoplasmic or nuclear localization (Schaufele et al., 2005). Error bars represent 2× SEM.

The FRET readout system applied was based on photobleaching of the acceptor and measuring the subsequential increase of the donor (abFRET; Bastiaens and Jovin, 1996; Bastiaens et al., 1996; Kenworthy, 2001; Fig. S2 A, available at http://www.jcb.org/cgi/content/full/jcb.200609178/DC1). In the presence of R1881, cells with a low expression (Fig. S1) of either the wild-type YFP-AR-CFP or the non–DNA binding mutant YFP-AR(A573D)-CFP showed a considerable increase in CFP fluorescence after acceptor bleaching, whereas only a small increase was observed in the N/C interaction–deficient mutant YFP-AR(F23,27A/L26A)-CFP (Fig. 1 E). In addition, abFRET was not observed in the absence of agonistic ligand (Fig. S2 B). These data indicate that the measured abFRET represents interaction of the FQNLF motif in the AR NTD with the ligand induced groove in the LBD. This was further corroborated by in vitro spectroscopy showing that FRET was strongly reduced by the addition of FQNLF peptide motifs, which compete with the AR N terminus for interaction with the C-terminal LBD, in lysates of cells expressing YFP-AR-CFP (Fig. 1 F). This reduction in FRET signal was not observed when, instead of FQNLF motifs, noncompeting LQNLL peptide motifs were added to the lysates (Fig. 1 F), confirming that the observed FRET is due to N/C interaction. Finally, extending previous data (Schaufele et al., 2005), confocal time-lapse microscopy of living cells stably expressing YFP-AR-CFP showed that the YFP/CFP ratio considerably increased immediately after the addition of hormone, followed by efficient translocation to the nucleus (Fig. 1 G). In contrast, the N/C interaction–deficient mutant YFP-AR(F23,27A/L26A)-CFP showed only a small increase in YFP/CFP ratio (Fig. S3). Based on these data, it can be concluded that the FRET measured in the double-tagged YFP-AR-CFP represents N/C interaction.

Simultaneous FRAP and FRET enables analysis of the mobility of interacting molecules

We developed a method based on simultaneous measurement of FRAP and FRET to study the mobility of interacting molecules. In this method, FRET-donor (CFP) and FRET-acceptor (YFP) fluorescence are simultaneously measured at regular time intervals after irreversibly photobleaching the acceptor in a defined subregion of the nucleus. Donor fluorescence increase after acceptor photobleaching and subsequent decrease because of diffusion (donor-FRAP) reflects the mobility of only the interacting molecules (Fig. 2 A). In contrast, acceptor fluorescence redistribution after acceptor bleaching (acceptor-FRAP) reveals the mobility of the total pool of both interacting and noninteracting molecules, similar to a conventional FRAP experiment (Houtsmuller et al., 1999; Houtsmuller and Vermeulen, 2001). Importantly, comparison of donor-FRAP and acceptor-FRAP curves allows us to distinguish the mobility (and immobilization) of the subpopulations of interacting and noninteracting proteins.

First, the method was validated in Hep3B cells expressing either a CFP-YFP fusion protein or separate CFPs and YFPs (Fig. 2, B and C). In brief, a narrow strip spanning the nucleus was scanned at 458 nm excitation with short intervals (100 ms) at low laser power (YFP is sufficiently excited at this wavelength; Fig. S4 A, available at http://www.jcb.org/cgi/content/full/jcb.200609178/DC1). Fluorescence intensities of the donor (CFP) and acceptor (YFP) were recorded simultaneously. After 40 scans, a high-intensity, 100-ms bleach pulse at 514 nm was applied to specifically photobleach YFPs inside the strip (CFP was not bleached by the bleach pulse; Fig. S4 B). Subsequently, scanning of the bleached strip was continued at 458 nm at low laser intensity. Acceptor (YFP) fluorescence in the strip was considerably reduced after bleaching and recovered at a velocity expected (Farla et al., 2005) for molecules the size of the fusion proteins (Fig. 2, B and C). In parallel, donor fluorescence in the bleached strip increased immediately after acceptor bleaching and decreased at a similar rate compared with the increase of YFP fluorescence (Fig. 2). The observed CFP increase and

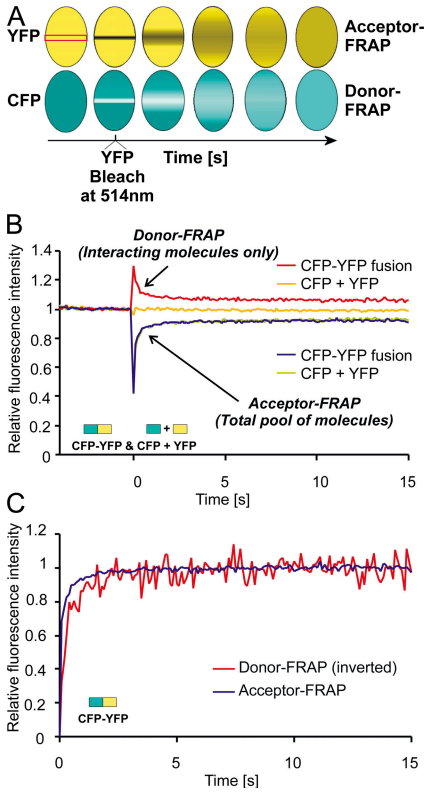

Figure 2. **Simultaneous FRAP and FRET measurements to separately determine the mobility of interacting and noninteracting CFP- and YFP-tagged proteins in a single-cell nucleus.** (A) Schematic representation of the method. A 100-ms high-intensity bleach pulse at 514 nm is applied to irreversibly photobleach YFPs in a narrow strip spanning the nucleus. Subsequently, redistribution of YFP and CFP fluorescence is recorded at 100-ms intervals (at 458 nm). Donor (CFP) emission (increased because of unquenching as a result of acceptor [YFP] bleaching) represents the mobility of interacting molecules only (donor-FRAP). Acceptor emission represents the total pool of YFP-tagged molecules irrespective of interaction (acceptor-FRAP). (B) Graph showing CFP and YFP fluorescence intensity in the bleached strip plotted against time. Experiments were performed in Hep3B cells expressing CFP-YFP fusions (red line indicates CFP fluorescence [donor-FRAP], and blue line indicates YFP fluorescence [acceptor-FRAP]), or in Hep3B cells expressing separate CFPs and YFPs (yellow line indicates CFP, and green line indicates YFP; $n = 30$). (C) Inverted donor-FRAP (red line) and acceptor-FRAP (blue line) plotted against time, showing similar kinetics. The curves were normalized by calculating $I_{norm} = (I_{raw} - I_0)/(I_{final} - I_0)$, where I_0 and I_{final} are the fluorescence intensities immediately after the bleach and after complete recovery, respectively.

subsequent decrease was not due to an artifact of YFP or CFP fluorescent properties, as cotransfected separate YFPs and CFPs, as well as ARs tagged with YFP or CFP only, did not show a donor-FRAP signal (Fig. 2 B and Fig. S4).

AR N/C interactions are abolished when ARs are bound to DNA

We performed simultaneous FRAP and FRET experiments to investigate the AR N/C interaction. As a control experiment, we tested an AR tagged at the N terminus with the CFP-YFP fusion protein. FRET will occur in these fusion proteins independent of the N/C interaction, as CFP and YFP are always in proximity. Donor-FRAP and acceptor-FRAP of CFP-YFP-AR both showed the same redistribution kinetics (Fig. 3, A and B), which are slower than that of the CFP-YFP fusion alone (Fig. 2 C) because of transient binding to DNA of wild-type ARs (Farla et al., 2004, 2005; Fig. 3, A and B). In sharp contrast, donor-FRAP of the two-sided double-tagged YFP-AR-CFP (representing solely the mobility of N/C-interacting ARs) was considerably faster than the corresponding acceptor-FRAP (representing the mobility of the total AR pool; Fig. 3 C). The difference between donor-FRAP and acceptor-FRAP was not observed for the double-tagged non–DNA binding AR mutant (YFP-AR[A573D]-CFP; Fig. 3 D). Moreover, the YFP-AR-CFP donor-FRAP curve (Fig. 3 C) showed fast kinetics similar to both donor-FRAP and acceptor-FRAP curves of the non–DNA binding AR mutant (Fig. 3 D). These data strongly suggest that N/C interactions of the wild-type AR occur mainly in the mobile pool and are abolished when ARs are transiently immobilized in a DNA binding–dependent fashion.

AR N/C interaction is reduced inside speckles

To further explore the observation that N/C interaction is reduced when ARs are transiently immobilized, we determined the spatial distribution of N/C-interacting and non–N/C-interacting ARs by high-resolution confocal ratio imaging of YFP-AR-CFP. Because YFP and CFP are present in the same quantity in cells expressing YFP-AR-CFP protein, these can be analyzed by straightforward ratio imaging. In brief, ratio images of cells expressing YFP-AR-CFP, CFP-YFP-AR, and the non–DNA binding YFP-AR(A537D)-CFP were obtained by calculating for each pixel the ratio between the YFP and CFP emission intensity. Subsequently, the nuclei were divided into three areas based on the mean fluorescence intensity of the entire nuclear area and corresponding standard deviation. In YFP-AR-CFP images, pixels with intensities higher than the mean plus two times the standard deviation (4.1% of total area; Fig. 4 A, red bars) coincided largely with the area that is usually referred to as a speckled or focal pattern, whereas pixels with lower intensities coincided largely with the region outside the speckled pattern (Fig. 4, A and B; for image analysis, see Materials and methods). The mean YFP/CFP ratio in each region was then calculated and expressed relative to the mean ratio in corresponding regions in CFP-YFP-AR with a similar intensity (see Materials and methods). Cells expressing CFP-YFP-AR provide an ideal control to correct for potential imaging artifacts because the ratio should be independent of AR folding and absolute fluorescence intensity. The wild-type YFP-AR-CFP showed a significantly reduced YFP/CFP ratio in the speckles compared with the region outside the speckles (Fig. 4 E; $P = 0.0002$; see Materials and methods), whereas no correlation is found for the non–DNA binding YFP-AR(A537D)-CFP, which showed a homogeneous distribution (Fig. 4, C, D, and F). Apparently, the concentration of non–N/C-interacting ARs is highest inside speckles.

AR speckles partially overlap sites of active transcription

The results described in the previous paragraphs, suggesting that N/C interactions are abolished when AR is immobilized because of DNA binding and that N/C interactions are decreased

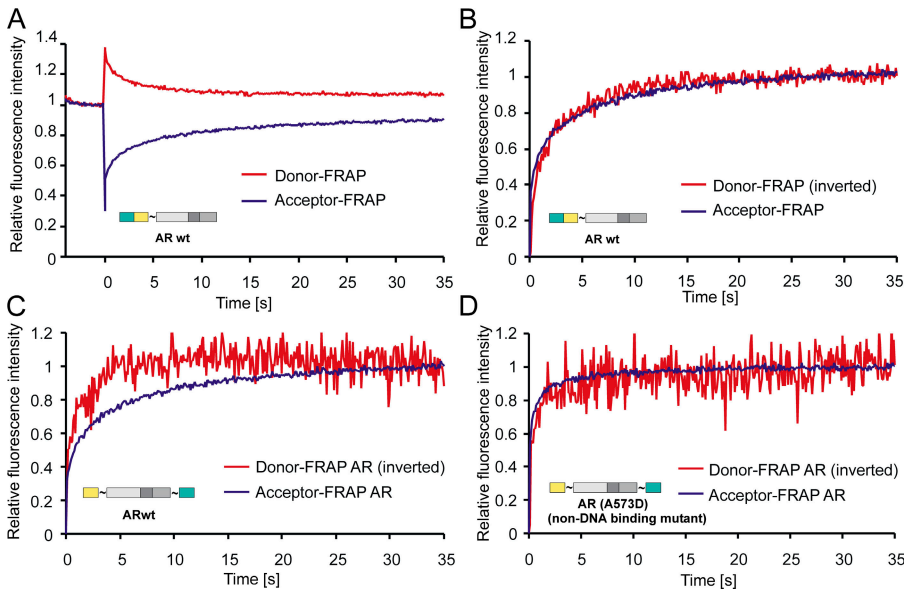

Figure 3. **Simultaneous FRAP and FRET measurements in Hep3B cells expressing CFP-YFP-AR or wild-type or mutant YFP-AR-CFP.** (A and B) Donor-FRAP (red line) and acceptor-FRAP (blue line) curves of ARs tagged at the N terminus with the CFP-YFP fusion (CFP-YFP-AR) also show similar redistribution kinetics, but slower than the CFP-YFP fusion (Fig. 2; $n = 30$). (C) Donor-FRAP (red line) and acceptor-FRAP (blue line) recorded in Hep3B cells expressing YFP-AR-CFP. The donor-FRAP curve (representing the mobility of N/C-interacting ARs only) shows faster recovery than the corresponding acceptor-FRAP curve (representing mobility of the total pool of AR; $n = 45$). (D) Donor-FRAP (red line) and acceptor-FRAP (blue line) curves of the non–DNA-binding YFP-AR(A573D)-CFP are rapid and similar to each other and to the donor-FRAP curve of YFP-AR-CFP (C), suggesting that N/C interactions occur only when ARs are mobile ($n = 45$). The curves in B, C, and D were normalized by calculating $I_{norm} = (I_{raw} - I_0)/(I_{final} - I_0)$, where I_0 and I_{final} are the fluorescence intensities immediately after the bleach and after complete recovery, respectively.

inside speckles, prompted us to investigate whether the AR speckled pattern is correlated to the distribution of sites of active transcription. Previously, it was shown, using 5-bromo-uridine-5′-triphosphate (BrUTP) incorporation in nascent RNA and immunofluorescence (Jackson et al., 1993; Wansink et al., 1993), that progesterone receptor (Arnett-Mansfield et al., 2007), glucocorticoid receptors (Van Steensel et al., 1995), and several other transcription factors (BRG1, TFIIH, Oct1, and E2F-1; Grande et al., 1997) do not show a complete, but rather a partial, overlap with active sites of transcription (nascent RNA). Using the same approach (see Materials and methods), we were able to detect sites of transcription in Hep3B cells stably expressing GFP-AR at physiological levels (Farla et al., 2005). Newly incorporated BrUTP was detected by immunofluorescence using Cy3, which is excited at 543 nm excitation, and GFP-AR was detected by 488 nm excitation. 60 dual channel images were recorded at a configuration at which no cross talk occurred (Fig. 5, A and B). Interestingly, visual analysis showed only a partial overlap between the AR speckles and sites of active transcription (Fig. 5, C [right] and D [closed vs. open arrows]). We quantified this observation by image analysis in which AR speckles and areas of active transcription were identified based on the mean fluorescence intensity of the entire nuclear area and corresponding standard deviation. Similar to the ratio imaging analysis (Fig. 4), where we used the same procedure to identify AR speckles (see the previous paragraph), pixels in the GFP-AR image with intensities higher than the mean plus two times the standard deviation coincided largely with AR speckles (Fig. 5 E, left and right). In the Cy3-labeled BrUTP image, pixels with intensities higher than the mean plus two times the standard deviation were defined to be hot spots of transcription (Fig. 5 E, middle and right). The centers of, on average, 110 AR speckles and 130 hot spots of transcription per nucleus were then determined. Subsequently, the distances between each AR speckle and the closest hot spot of transcription were determined and compared with a randomly distributed set consisting of an equal number of spots with the same size distribution as the measured hot spots of transcription, taking care that the random spots were not in the nucleoli or outside the nucleus. The number of AR speckles at relatively short distance (<350 nm; Fig. 5 F, first five columns) to the nearest BrUTP spot was significantly higher compared with what is expected on the basis of a random

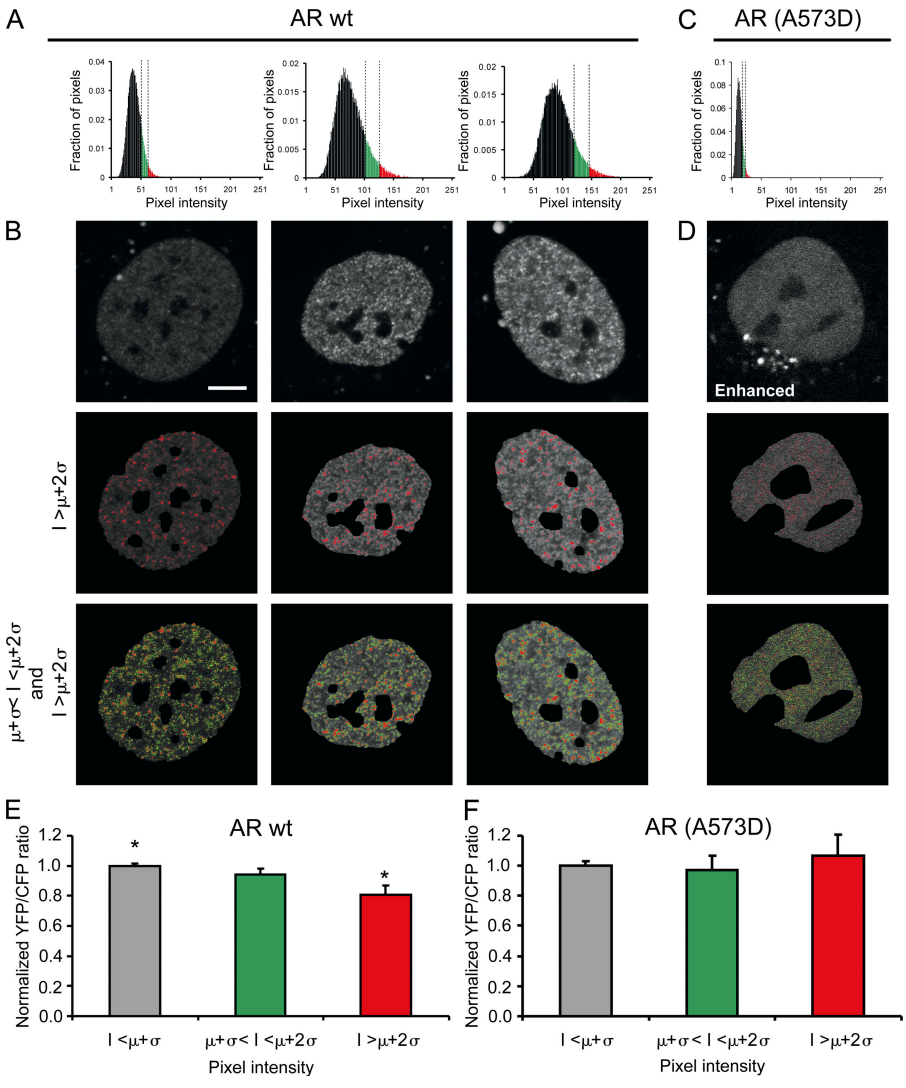

Figure 4. **YFP-CFP ratio imaging on Hep3B cells expressing wild-type or mutant YFP-AR-CFP.** (A) Fluorescence intensity distributions of nuclei expressing wild-type YFP-AR-CFP. For FRET analysis, the histograms were used to subdivide the nucleus in three areas based on mean intensity (μ) and standard deviation (σ): pixel intensity $I < \mu + \sigma$ (black bars; 81.3% of total area), $\mu + \sigma < I < \mu + 2\sigma$ (green bars; 14.6%), and $I > \mu + 2\sigma$ (red bars; 4.1%). (B, top) Confocal images of the nuclei corresponding to the histograms in A. Bar, 5 μm. (middle) Same nuclei (without background and regions with $I > \mu + 2\sigma$ indicated in red). (bottom) Regions with $\mu + \sigma < I < \mu + 2\sigma$ indicated in green. Using the relative intensity threshold $> \mu + 2\sigma$ specifically selects high-intensity regions that coincide largely with the well-described nuclear foci that give rise to a speckled pattern (Farla et al., 2005). (C and D) Intensity distribution and confocal image of a nucleus expressing non–DNA binding mutant AR(A573D). Although pixels with an intensity $> \mu + 2\sigma$ are present, these are randomly distributed throughout the nucleus and do not form aggregates or speckles. Contrast and brightness of the AR(A573D) images are digitally enhanced for visualization purposes, not for analysis. (E and F) YFP/CFP ratio of cells expressing wild-type and non–DNA binding mutant YFP-AR(A573D)-CFP in the different relative pixel intensity categories (data are mean ± SEM of 100 and 20 cells measured in three and two independent experiments, respectively). Ratios in each category were normalized to corresponding categories measured in cells expressing CFP-YFP-AR with similar intensity. In wild-type AR (E), a lower YFP/CFP ratio is observed in the regions with higher intensity, indicating the loss of N/C interaction in speckles (*, P = 0.0002). This is not found for the AR(A573D) (F).

distribution (43 ± 5 measured vs. 24 ± 2 random spots; P = 0.00025; Fig. 5 F). Moreover, the largest relative difference between measured and random was highest at the closest detectable distance. In addition, the number of AR speckles that showed overlap with the nearest hot spot of transcription was significantly higher than expected when there would be no correlation between AR and nascent RNA distributions ($P = 5.0 \times 10^{-8}$; Fig. 5 G).

ARA54 cofactor fragments preferentially interact with DNA-bound ARs

The strongly reduced N/C interaction in the transient immobile AR fraction led us to hypothesize that AR coregulators containing FxxLF motifs may gain access more easily to this fraction, as no competition with the N-terminal AR FQNLF motif is expected to occur. We tested this hypothesis using YFP-tagged fragments of the cofactor ARA54, containing an FNRLF motif. ARA54 and ARA54 fragments containing the FNRLF motif were previously shown to display a strong interaction with the AR LBD (Kang et al., 1999; He et al., 2002; Van de Wijngaart et al., 2006). In agreement with this hypothesis, abFRET between the single-tagged wild-type AR-CFP and YFP-ARA54 fragments was significantly higher (P = 0.003; see Materials and methods) than that of the non–DNA binding mutant AR(A573D)-CFP with YFP-ARA54, suggesting that interactions between AR and ARA54 fragments are significantly enhanced when ARs are bound to DNA (Fig. 6 A, left). To further test the hypothesis that AR N/C interactions are responsible for blocking coregulator interactions, we performed the same experiment using the N/C interaction–deficient mutant AR(F23,27A/L26A)-CFP. In contrast to wild-type AR, no difference in FRET with the ARA54 fragments was observed for the mutant and its non–DNA binding variant AR(F23,27A/L26A/A573D)-CFP. Moreover, FRET was higher than that of the N/C interaction–proficient wild-type ARs (P = 0.042) and much higher than the N/C interaction–proficient non–DNA binding mutant (Fig. 6 A, left). No FRET was found between any of the AR mutants and free YFP (Fig. 6 A, right). These data are in agreement with a model in which YFP-ARA54 fragments bind preferentially to ARs lacking N/C interaction, i.e., either N/C interaction–deficient AR(F23,27A/L26A) mutants

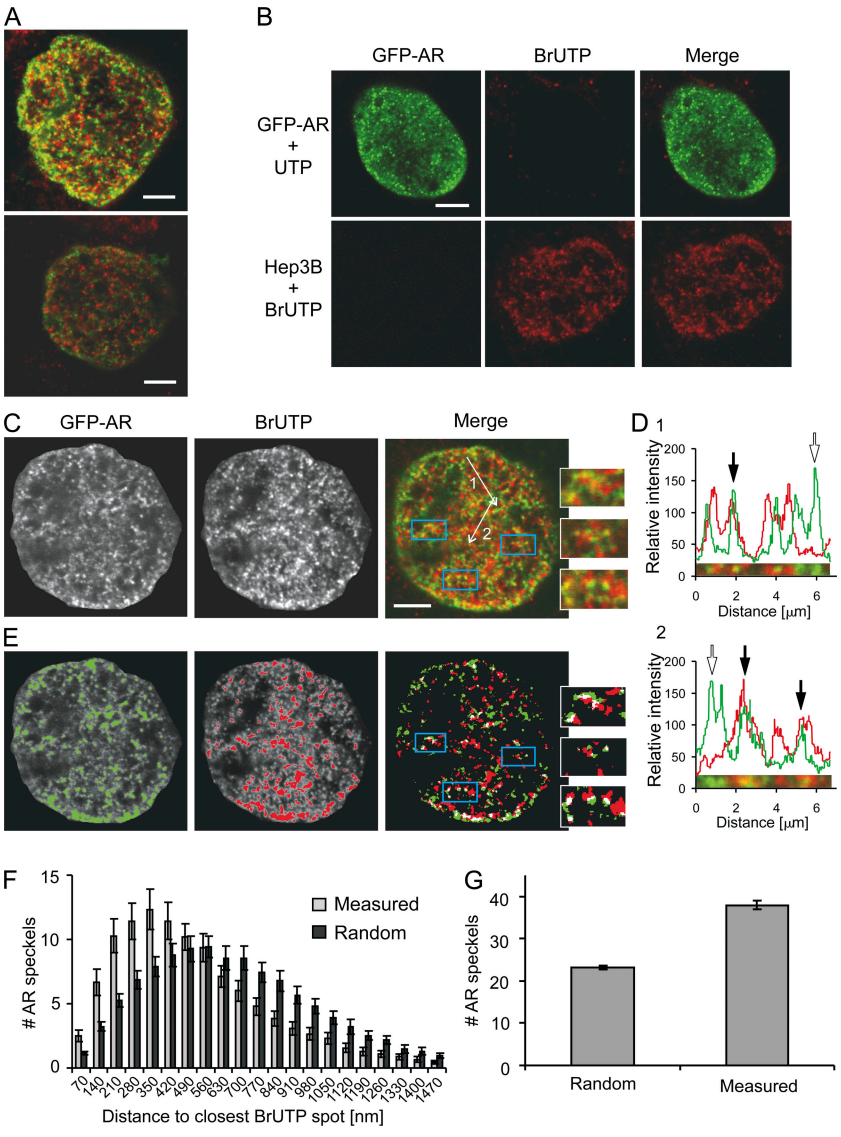

Figure 5. **AR speckles and hot spots of transcription.** (A) Distribution of GFP-AR (green) and sites of BrUTP incorporation (red) in stably transfected Hep-3B cells (Farla et al., 2004). Sites of BrUTP incorporation were visualized by immunofluorescence. (B) The fluorescent signals were monitored by sequential imaging of the GFP and Cy3 channels using confocal microscopy at a configuration at which no cross talk of signals occurred. (C) Confocal images of a fixed Hep3B cell that stably expressed GFP-AR (green) and shows incorporated BrUTP staining (red). A partial overlap of the AR speckled pattern with sites of transcription can be seen (right and insets). White lines indicate the position of the line scans in D. Bars, 5 μm. (D) Line scans at the indicated position in C of the AR (green) and the BrUTP signal (red). Some but not all peaks coincided, indicating partial colocalization of some of the AR speckles with sites of transcription. Closed arrows indicate coinciding peaks, and open arrows indicate AR speckles without a colocalized transcription site. (E) Images of AR and BrUTP thresholded similar to YFP-AR-CFP in Fig. 4. In both the GFP-AR (GFP; green) and BrUTP (Cy3; red) channels, regions with an intensity $I > \mu + 2\sigma$ and are indicated (two left panels). A merged image of the selected regions in both channels (right) shows the partial overlap (white) in the regions with an intensity $I > \mu + 2\sigma$. The insets represent the same regions as in C. (F) Distribution of distances between AR speckles and the nearest BrUTP spot (light gray bars) or randomly distributed spots (dark gray bars; $n = 68$). The number of AR speckles at relatively short distance (<350 nm) to the nearest BrUTP spot was significantly higher than expected on the basis of random distribution (P = 0.00025) and highest at the closest detectable distance. (G) Mean number of AR speckles overlapping with the nearest UTP spot ($n = 68$). The number of AR speckles partially overlapping BrUTP spots is larger than expected on the basis of a random distribution ($P = 5.0 \times 10^{-8}$).

or wild-type ARs transiently immobilized as a result of DNA binding.

To investigate this more extensively, we repeated the simultaneous FRAP and FRET measurements in living Hep3B cells expressing YFP-AR-CFP, now in the presence of cotransfected YFP-ARA54 fragments. The addition of YFP-ARA54 fragments considerably reduced the kinetics of the donor-FRAP curve compared with YFP-AR-CFP in absence of YFP-ARA54 fragments (Fig. 6 B). This is explained by the fact that in this experimental setup not only the N/C-interacting mobile ARs, but also the non–N/C-interacting immobile ARs, show FRET, now between AR C-terminal domain and the YFP-ARA54 fragments (which binds to the C-terminal domain instead of the YFP-tagged N-terminal domain of immobile YFP-AR-CFP). This indicates that the ARA54 fragments preferably interact with the C terminus of the AR when it is transiently immobilized because of DNA binding when the N-terminal FQNLF motif does not compete for interaction with the C-terminal domain.

In summary, the abFRET data (Fig. 6 A) show that ARA54 fragments interact more frequently with wild-type AR than with the non–DNA binding mutant. The simultaneous FRAP and FRET analysis (Fig. 6 B) suggests that this is because ARA54 fragments gain access more easily to the C-terminal LBD of the wild-type ARs when there is no, or less, competition with the NTD. This occurs either when wild-type ARs are transiently immobilized in a DNA binding–dependent manner (Fig. 3 C) or when the N/C interaction is disrupted (Fig. 6 A).

Discussion

Activity of SRs is not only regulated by ligand binding but also by interacting cofactors. The best-described binding site for SR coregulators is the hydrophobic cleft in the LBD to which LxxLL motifs can bind. The AR LBD is unique in its preference for the interaction with cofactors carrying FxxLF motifs rather than LxxLL motifs (Dubbink et al., 2004; Hur et al., 2004). The AR itself also contains an FQNLF motif in the N-terminal domain, enabling interaction with the LBD (N/C interaction; Doesburg et al., 1997; He et al., 2000). The potential competition between the AR N-terminal FQNLF motif and similar motifs in cofactors for interaction with the LBD raises questions regarding the role of the N/C interaction in orchestrating cofactor interactions. To study AR N/C interactions in living cells, we tagged the AR at the N and C termini with YFP and CFP, respectively, or with CFP alone, and applied FRET and simultaneous FRET and FRAP experiments. In addition, to investigate cofactor interactions, we tagged ARA54 fragments containing an FNRLF motif with YFP. The presence of the tags had no effect on AR localization and hormone-induced nuclear translocation (Fig. 1, D and G) and only limited effect on the transactivation function of the AR (Fig. 1 C). Acceptor photobleaching FRET assays on living cells and in vitro competition experiments using FxxLF- and LxxLL-peptide motifs demonstrated that FRET represents N/C interaction (Fig. 1, E and F).

Previously, using FRAP assays, we and others have shown that the mobility of ARs is reduced compared with the mobility of non–DNA binding AR(A573D) mutants (Farla et al., 2004), as well as antagonist-bound ARs (Farla et al., 2005). In addition, the observed hormone-induced slow down of AR mobility was always accompanied by the formation of a speckled distribution pattern in the nucleus, suggesting that ARs transiently immobilize in speckles. We have now shown using combined FRET and FRAP analysis that, surprisingly, the mobility of the pool of N/C-interacting ARs is not reduced in the presence of hormone and that, consequently, the pool of non–N/C-interacting ARs is responsible for the observed overall slow down of AR mobility. This suggests that the N/C interaction is largely lost when ARs are transiently immobilized, most likely because of DNA binding (Fig. 3 C). This was confirmed by high-resolution ratio imaging showing that FRET is reduced inside speckles (Fig. 4 E).

The loss of N/C interaction in immobilized ARs suggests that the C-terminal hydrophobic groove, to which FxxLF motifs

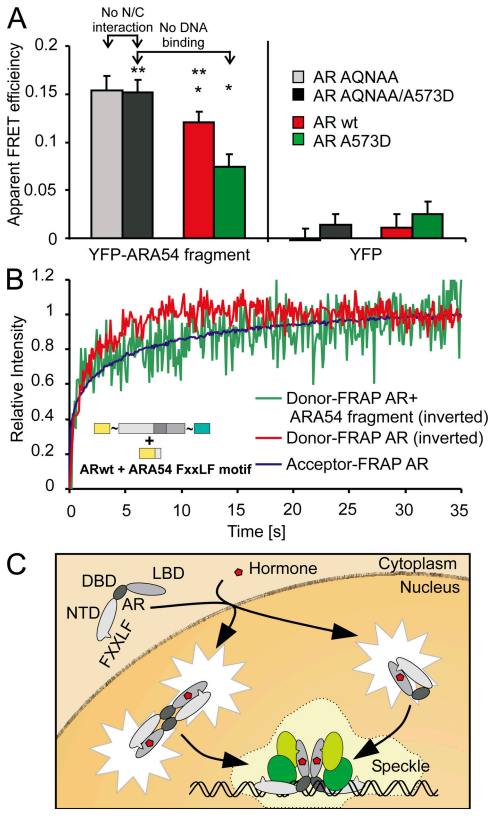

Figure 6. **Interaction of ARA54 cofactor fragments with the AR.** (A) AbFRET between YFP-tagged ARA54 fragments and CFP-tagged wild-type AR (red bar) and three mutants: the non–DNA-binding mutant A573D (green bar), the N/C interaction–deficient AR(F23,27A/L26A; gray bar), and an AR carrying both mutations (black bar). Control experiments with free YFP are also shown (data are mean ± SEM of four independent experiments in which 15 cells were measured; *, P = 0.003; **, P = 0.042). (B) Donor-FRAP curve of cells expressing YFP-AR-CFP and YFP-ARA54 fragments (green line), showing considerably retarded mobility compared with donor-FRAP of YFP-AR-CFP only (red line) and similar to the acceptor-FRAP of YFP-AR-CFP only (blue line), suggesting that ARA54 fragments interact preferentially when ARs are transiently immobilized (n = 45). The curves were normalized by calculating $I_{norm} = (I_{raw} - I_0)/(I_{final} - I_0)$, where I_0 and I_{final} are the fluorescence intensities immediately after the bleach and after complete recovery, respectively. (C) Model of N/C and coregulator interactions of the AR. N/C interactions may be either inter- or intramolecular (Schaufele et al., 2005) but are disrupted when AR is bound to DNA, allowing interactions with coregulators.

can bind, is optimally accessible for coregulators when the ARs are bound to DNA. Our acceptor bleaching FRET experiments on YFP-tagged FNRLF fragments of the AR cofactor ARA54 and AR-CFP provide evidence that strongly supports this view. First, the experiments indicate that ARA54 fragments interact more frequently with the wild-type AR than with the non–DNA-binding AR mutants (A573D), whereas the non–N/C-interacting mutants of DNA binding and non–DNA binding ARs do not show this difference and interact more frequently than any of the N/C interaction–proficient ARs (Fig. 6 A). Moreover, when YFP-tagged ARA54 fragments are coexpressed with YFP-AR-CFP in a simultaneous FRET and FRAP assay, the mobility of the N/C-interacting pool is reduced (Fig. 6 B). This indicates that on top of the mobile N/C-interacting ARs, the immobile double-tagged ARs now show FRET because of their interaction with the YFP-tagged ARA54 fragments. The observed loss of N/C interaction in immobile ARs and frequent interactions of cofactor fragments with immobile ARs are in line with a scenario in which the AR itself dynamically regulates the time and place of interactions with coregulators by blocking the groove using its N-terminal FQNLF motif when not associated to DNA and allowing access of coregulators only after DNA binding (Fig. 6 C).

Because our data suggest that DNA binding occurs in speckles, the question arose whether these speckles also represent sites of active transcription. To investigate this, we performed BrUTP incorporation experiments on Hep3B cells stably expressing AR-GFP. Interestingly, visual as well as statistical analysis showed that although speckles are closer to sites of active transcription than expected on the basis of a random distribution, AR and transcription hot spots only partially overlap (Fig. 5), suggesting that DNA binding of the AR does not always result in the formation of productive transcription complexes. Several lines of previous evidence are in agreement with these observations. First, it has been shown that progesterone receptor (Arnett-Mansfield et al., 2007), glucocorticoid receptors (Van Steensel et al., 1995), and several other transcription factors (BRG1, TFIIH, Oct1, and E2F-1; Grande et al., 1997) showed only a partial correlation with active sites of transcription. Second, recent data on estrogen receptors using chromatin immunoprecipitation on chip assays suggested that SRs have many more binding sites (~3,600) in the genome than expected on the basis of the estimated number of estrogen receptor–regulated genes, which probably is in the order of hundreds rather than thousands (Carroll et al., 2006). Third, it has been shown by chromatin immunoprecipitation that DNA binding of the estrogen receptor occurs in a cyclic pattern and that an initial cycle of binding only prepares promoters for transcription but does not result in a productive transcription complex (for review see Métivier et al., 2006). However, these nonproductive cycles were observed in cells shortly after application of the hormone. It remains questionable whether after longer exposure to hormone, as used in our experiments, promoters would be "shut down" and reactivated.

If not all immobile ARs are involved in active transcription, the question of what happens in speckles remains. It has frequently been suggested that many transcription factors, and other nuclear factors involved in DNA metabolism, bind transiently to DNA also at nonspecific sites, thereby scanning the DNA (Phair et al., 2004; Métivier et al., 2006). Possibly the majority of immobile ARs observed in our experiments are involved in such scanning activity. The interaction with cofactors may then play a role in identifying specific binding sites when encountered during scanning. In addition, it is not excluded that part of the speckles represents some sort of storage site. However, as non–DNA-binding mutants do not form speckles and move freely through the nucleus, such a model suggests that the DBD is also involved in storage.

In conclusion, we have used a novel combination of FRAP and FRET to investigate interactions of the AR in living cells and provided evidence that AR N/C interactions are involved in the spatiotemporal regulation of interactions with coregulators. The FRET/FRAP assay provides a novel tool to separately investigate the dynamics of interacting and noninteracting molecules. This opens up a multitude of possibilities to investigate the molecular mechanisms underlying not only the regulation of gene transcription but also that of other DNA transacting systems, such as DNA repair and replication.

Materials and methods

Constructs

The cDNA construct encoding N-terminally YFP-tagged AR was generated by replacing EGFP in pGFP-$(GA)_6$-AR (Farla et al., 2004) by EYFP-C1 (CLONTECH Laboratories, Inc.). The C-terminally CFP-tagged AR was generated by replacing EGFP by ECFP-N3 (CLONTECH Laboratories, Inc.) in pAR-$(GA)_6$-EGFP in which two AR fragments from pcDNA-AR0mcs (lacking the AR stop codon; Sui et al., 1999) and pAR0 (Brinkmann et al., 1989), respectively, were sequentially inserted in EGFP-N3 (CLONTECH Laboratories, Inc.) followed by the introduction of a spacer sequence coding for a $(Gly\text{-}Ala)_6$ stretch. The construct coding for double-tagged AR (pYFP-$[GA]_6$-AR-$[GA]_6$-CFP) was generated by combining a fragment of N-terminally YFP-tagged AR pYFP-$(GA)_6$-AR with a fragment of C-terminally CFP-tagged AR pAR-$(GA)_6$-CFP. The F23,27A/L26A variants were generated by QuikChange (Stratagene) mutagenesis using primers 5′-ACCTACCGAGGAGCTGCACAGAATGCTGCACAGAGCGTGCGCGAA-3′ and 5′-TTCGCGCACGCTCTGTGCAGCATTCTGTGCAGCTCCTCGGTAGGT-3′. To generate the A573D variants, the AR DBDs of pYFP-AR-CFP and pAR-$(GA)_6$-CFP were replaced by a pGFP-AR(A573D) (Farla et al., 2004) fragment containing the AR DBD (A573D) mutation. EYFP in pYFP-$(GA)_6$-AR was replaced by an ECFP-EYFP fusion to obtain pCFP-YFP-(GA)6-AR. The YFP-tagged ARA54 peptide construct was obtained by annealing the primers 5′-GATCGACCCTGGTTCACCATGTTTTAACCGGCTGTTTTATGCTGTGGATGTTG-3′ and 5′-AATTCAACATCCACAGCATAAAACAGCCGGTTAAAACATGGTGAACCAGGGTC-3′ containing the FNRLF motif and inserting the fragment in pEYFP-C2 (CLONTECH Laboratories, Inc.). Structures of novel constructs were verified by appropriate restriction digestions and by sequencing. Sizes of expressed proteins were verified by Western blotting. pCYFP encoding the ECFP-EYFP fusion was provided by C. Gazin (Hôpital Saint-Louis, Paris, France). The $(ARE)_2$-TATA Luc reporter was a gift from G. Jenster (Josephine Nefkens Institute, Rotterdam, Netherlands).

Cell culture, transfections, and luciferase assay

2 d before microscopic analyses, Hep3B cells were grown on glass coverslips in 6-well plates in α-MEM (Cambrex) supplemented with 5% FBS (HyClone), 2 mM L-glutamine, 100 U/ml penicillin, and 100 μg/ml streptomycin. At least 4 h before transfection, the medium was substituted by medium containing 5% dextran charcoal stripped FBS. Transfections were performed with 1 μg/well AR or CFP-YFP expression constructs or 0.5 μg/well empty vector in FuGENE6 (Roche) transfection medium. In the indicated experiments, YFP-tagged ARA54 peptide expression constructs (0.5 μg/well) were added. 4 h after transfection, the medium was replaced by medium with 5% dextran charcoal stripped FBS with or without 100 nM R1881. Hep3B cells stably expressing AR constructs were subjected to the same medium-replacement schedule.

For the AR transactivation experiments, Hep3B cells were cultured in 24-well plates on α-MEM supplemented with 5% dextran charcoal stripped FBS in the presence or absence of 100 nM R1881 and transfected using 50 ng AR expression construct and 100 ng $(ARE)_2$TATA Luc reporter. 24 h after transfection, cells were lysed and luciferase activity was measured in a luminometer (Fluoroscan Ascent FL; Labsystems Oy). Light emission was recorded during 5 s, after a delay of 2 s.

Western blot analysis

Hep3B cells were cultured and transfected in 6-well plates. 24 h after transfection, cells were washed twice in ice-cold PBS and lysed in 200 μl Laemmli sample buffer (50 mM Tris-HCl, pH 6.8, 10% glycerol, 2% SDS, 10 mM DTT, and 0.001% Bromophenol blue). After boiling for 5 min, a 5-μl sample was separated on a 10% SDS-polyacrylamide gel and blotted to Nitrocellulose Transfer Membrane (Protran; Schleicher and Schuell). Blots were incubated with anti-AR (1:2,000; mouse monoclonal F34.4.1) or anti–β-actin (1:10,000; mouse monoclonal anti–β-actin [Sigma-Aldrich]) and subsequently incubated with HRP-conjugated goat anti–mouse antibody (Dako-Cytomation). Proteins were visualized using Super Signal West Pico Luminol solution (Pierce Chemical Co.), followed by exposure to x-ray film.

Confocal imaging and FRET acceptor photobleaching

Live-cell and immunofluorescence imaging was performed using a confocal laser-scanning microscope (LSM510; Carl Zeiss MicroImaging, Inc.) equipped with a Plan-Neofluar 40×/1.3 NA oil objective (Carl Zeiss MicroImaging, Inc.) at a lateral resolution of 100 nm (FRET acceptor bleaching) or 70 nm (immunofluorescence). An argon laser was used for excitation of CFP, GFP, and YFP at 458, 488, and 514 nm, respectively, and a He/Ne laser was used to excite Cy3 at 543 nm.

Interactions between either the N- and C-terminal domain of the YFP-AR-CFP or between AR-CFP and YFP-ARA54 were assessed using acceptor photobleaching. For this, YFP and CFP images were collected sequentially before photobleaching of the acceptor. CFP was excited at 458 nm at moderate laser power, and emission was detected using a 470–500 nm bandpass emission filter. YFP was excited at 514 nm at moderate laser power, and emission was detected using a 560-nm longpass emission filter. After image collection, YFP in the nucleus was bleached by scanning a nuclear region of ~100 μm^2 25 times at 514 nm at high laser power, covering the largest part of the nucleus. After photobleaching, a second YFP and CFP image pair was collected. Apparent FRET efficiency was estimated (correcting for the amount of YFP bleached) using the equation $abFRET = ([CFP_{after} - CFP_{before}] \times YFP_{before})/([YFP_{before} - YFP_{after}] \times CFP_{after})$, where CFP_{before} and YFP_{before} are the mean prebleach fluorescence intensities of CFP and YFP, respectively, in the area to be bleached (after background subtraction), and CFP_{after} and YFP_{after} are the mean postbleach fluorescence intensities of CFP and YFP, respectively, in the bleached area. The apparent FRET efficiency was finally expressed relative to control measurements in cells expressing either free CFP and YFP ($abFRET_0$) or the CFP-YFP fusion protein ($abFRET_{CFP\text{-}YFP\ fusion}$): apparent FRET efficiency = $(abFRET - abFRET_0)/(abFRET_{CFP\text{-}YFP\ fusion} - abFRET_0)$. For statistical analysis, the abFRET datasets were tested for normality using the Kolmogorov-Smirnov test, and datasets were compared using the one-tailed *t* test.

For high-resolution immunofluorescent imaging of BrUTP incorporated into nascent RNA, Cy3 was excited at 543 nm at moderate laser power and emission was detected using a 560-nm longpass emission filter. GFP-AR was excited at 488 nm at moderate laser power, and emission was detected using a 505–530-nm bandpass emission filter. Cy3 and GFP images were recorded sequentially to avoid cross talk.

FRET spectroscopy

Spectroscopic analysis of crude cell lysates of cells expressing YFP-AR-CFP was performed on a fluorescence spectrophotometer (F-4500; Hitachi) by recording spectra at 425 nm excitation. The apparent FRET efficiency was calculated as the ratio of the emission intensities at 525 and 475 nm. Background fluorescence of lysates of cells not expressing YFP-AR-CFP prepared in the same way was negligible. Spectra were recorded of lysates in the absence and presence of 300 μM of synthesized peptides containing an FQNLF or LQNLL motif, respectively.

Simultaneous FRAP and FRET

To study the mobility of interacting proteins, a narrow strip spanning the nucleus was scanned at 458 nm excitation with short intervals (100 ms) at low laser power (YFP is sufficiently excited at this wavelength; Fig. S4 A). Fluorescence intensities of the donor (CFP) and acceptor (YFP) were recorded simultaneously using 470–500-nm bandpass and 560-nm longpass filters, respectively. After 40 scans, a high-intensity, 100-ms bleach pulse at 514 nm was applied to specifically photobleach YFPs inside the strip (CFP was not bleached by the bleach pulse; Fig. S4 B). Subsequently, scanning of the bleached strip was continued at 458 nm at low laser intensity. The curves are either normalized by calculating $I_{norm} = (I_{raw} - I_{bg})/(I_{pre} - I_{bg})$ or to compare donor-FRAP and acceptor-FRAP curves by calculating $I_{norm} = (I_{raw} - I_0)/(I_{final} - I_0)$, where I_{pre}, I_0, and I_{final} are the fluorescent intensities before, immediately after, the bleach and after complete recovery, respectively, and I_{bg} is the background intensity.

YFP/CFP ratio imaging

Because YFP and CFP are present in exactly the same quantity in cells expressing YFP-AR-CFP, ratio imaging can be applied to study the spatial distribution of ARs with and without N/C interaction. Local differences in YFP/CFP ratio within the nucleus of cells expressing YFP-AR-CFP will only be observed if the ratio between N/C-interacting ARs, showing a relatively high YFP/CFP ratio, and non–N/C-interacting ARs, showing a relatively low YFP/CFP ratio, are different. For high-resolution YFP/CFP ratio imaging, YFP and CFP were imaged simultaneously using a moderate excitation at 458 nm and a 470–500-nm bandpass emission filter for CFP and a 560-nm longpass emission filter for YFP. To reduce noise, eight times line averaging was used. Images were analyzed using the KS-400 image analysis package (Carl Zeiss MicroImaging, Inc.). Ratio images were obtained by calculating for each pixel $(I_{YFP} - I_{bg})/(I_{CFP} - I_{bg})$, where I_{YFP} and I_{CFP} are the intensities of the YFP and CFP emission, respectively, and I_{bg} is the background intensity. To obtain regions representing successive relative intensity ranges (Fig. 4), the mean of I_{YFP} and I_{CFP} was calculated for each pixel as $I_{mean} = (I_{YFP} + I_{CFP})/2$. The mean I_{mean} of each nucleus (termed μ in Fig. 4) and the standard deviation, σ, were then calculated after (manual) selection of the nuclear area and exclusion of the nucleoli (Fig. 4 B). The mean ratio in areas with pixel intensities $I_{mean} < \mu + \sigma$, $\mu + \sigma < I_{mean} < \mu + 2\sigma$ and $I_{mean} > \mu + 2\sigma$ were then first calculated for CFP-YFP-AR expressing cells. Because these molecules emit at a fixed YFP/CFP ratio irrespective of their conformation or local concentration, any difference in ratio in the three selected areas is due to imaging artifacts. Indeed, CFP/YFP ratio increased in CFP-YFP-AR expressing cells with low intensity and decreased in cells with high intensities probably because of the nonlinearity of the detectors. Therefore, data obtained from each cell expressing YFP-AR-CFP and the non–DNA-binding mutant YFP-AR(A573D)-CFP were expressed relative to the mean ratio measured in corresponding areas in seven cells expressing CFP-YFP-AR with similar expression level. For statistical analysis, the YFP/CFP ratio imaging datasets were tested for normality using the Kolmogorov-Smirnov test, and datasets were compared using the *t* test.

Immunofluorescent labeling of nascent RNA

Nascent RNA was detected by BrUTP incorporation in permeabilized living Hep3B cells stably expressing GFP-AR (Farla et al., 2004) according to Wansink et al. (1993). Cells were grown overnight on coverslips in medium containing 5% dextran charcoal stripped FBS in the presence of 100 nM R1881. The procedure of BrUTP incorporation has been previously described (Wansink et al., 1993). Cells were permeabilized in glycerol buffer (20 mM Tris HCl, 0.5 mM $MgCl_2$, 0.5 mM EGTA, 25% glycerol, and 1 mM PMSF) supplemented with 0.05% Triton X-100 and 10 U/ml RNAsin for 3 min. To allow BrUTP incorporation, permeabilized cells were incubated for 30 min at RT in synthesis buffer (100 nM Tris HCl, 5 nM $MgCl_2$, 0.5 mM EGTA, 200 mM KCl, 50% glycerol, 0.05 mM SAM, 20 U/ml RNAsin, and 0.5 mM PMSF) supplemented with 0.5 mM ATP, CTP, GTP, and BrUTP (or UTP as control; Sigma-Aldrich). Next, cells were fixed in 2% formaldehyde in PBS, incubated in 0.5% Triton X-100/PBS for 5 min and in 100 nM glycin/PBS for 10 min, each step followed by two PBS washes. After blocking with PBG (0.05% gelatin and 0.5% BSA in PBS), incorporated BrUTP was immunolabeled overnight with a rat anti-BrdU mAb (Seralab) diluted 1:500 in PBS at 4°C. After four washes with PBG, cells were incubated for 90 min at RT with biotin-conjugated sheep anti–rat IgG (Jackson ImmunoResearch Laboratories) 1:200 in PBS followed by four washes with PBG. The biotinylated antibody was then visualized with Cy3-conjugated streptavidin (Jackson ImmunoResearch Laboratories) 1:250 in PBS for 30 min at RT. After extensive washing with PBG and PBS, cells were embedded in Vectashield containing DAPI.

Online supplemental material

Fig. S1 shows YFP-AR-CFP expression analysis of cells used in the acceptor photobleaching FRET experiments and in the simultaneous FRAP and FRET measurements. Fig. S2 presents the validation of FRET measurements by acceptor photobleaching (abFRET) and shows the hormone dependency

of FRET measured in cells expressing YFP-AR-CFP. Fig. S3 shows the minimal YFP/CFP ratio change after the addition of R1881 in cells expressing YFP-AR(F23,27A/L26A)-CFP variant. Fig. S4 presents the control experiments for donor-FRAP and acceptor-FRAP on cells expressing YFP-AR and AR-CFP. Online supplemental material is available at http://www.jcb.org/cgi/content/full/jcb.200609178/DC1.

We thank Drs. J. Essers and R. Kanaar and for critically reading the manuscript.

This work is supported by grant DDHK 2002-2679 from the Dutch Cancer Society (KWF) and VIDI grant 016.046.371 from the Dutch Organisation for Scientific Research (NWO).

Submitted: 28 September 2006
Accepted: 12 March 2007

References

Agresti, A., P. Scaffidi, A. Riva, V.R. Caiolfa, and M.E. Bianchi. 2005. GR and HMGB1 interact only within chromatin and influence each other's residence time. *Mol. Cell.* 18:109–121.

Arnett-Mansfield, R.L., J.D. Graham, A.R. Hanson, P.A. Mote, A. Gompel, L.L. Scurr, N. Gava, A. de Fazio, and C.L. Clarke. 2007. Focal subnuclear distribution of progesterone receptor is ligand dependent and associated with transcriptional activity. *Mol. Endocrinol.* 21:14–29.

Bastiaens, P.I.H., and T.M. Jovin. 1996. Microspectroscopic imaging tracks the intracellular processing of a signal transduction protein: fluorescent-labeled protein kinase C beta I. *Proc. Natl. Acad. Sci. USA.* 93:8407–8412.

Bastiaens, P.I.H., I.V. Majoul, P.J. Verveer, H.-D. Söling, and T.M. Jovin. 1996. Imaging the intracellular trafficking and state of the AB5 quaternary structure of cholera toxin. *EMBO J.* 15:4246–4253.

Brinkmann, A.O., P.W. Faber, H.C.J. van Rooij, G.G.J.M. Kuiper, C. Ris, P. Klaassen, J.A.G.M. van der Korput, M.M. Voorhorst, J.H. van Laar, E. Mulder, and J. Trapman. 1989. The human androgen receptor: domain structure, genomic organization and regulation of expression. *J. Steroid Biochem.* 34:307–310.

Carroll, J.S., C.A. Meyer, J. Song, W. Li, T.R. Geistlinger, J. Eeckhoute, A.S. Brodsky, E.K. Keeton, K.C. Fertuck, G.F. Hall, et al. 2006. Genome-wide analysis of estrogen receptor binding sites. *Nat. Genet.* 38:1289–1297.

Claessens, F., G. Verrijdt, E. Schoenmakers, A. Haelens, B. Peeters, G. Verhoeven, and W. Rombauts. 2001. Selective DNA binding by the androgen receptor as a mechanism for hormone-specific gene regulation. *J. Steroid Biochem. Mol. Biol.* 76:23–30.

Cleutjens, K.B.J.M., H.A.G.M. van der Korput, C.C.E.M. van Eekelen, H.C.J. van Rooij, P.W. Faber, and J. Trapman. 1997. An androgen response element in a far upstream enhancer region is essential for high, androgen-regulated activity of the prostate-specific antigen promoter. *Mol. Endocrinol.* 11:148–161.

Doesburg, P., C.W. Kuil, C.A. Berrevoets, K. Steketee, P.W. Faber, E. Mulder, A.O. Brinkmann, and J. Trapman. 1997. Functional in vivo interaction between the amino-terminal, transactivation domain and the ligand binding domain of the androgen receptor. *Biochemistry.* 36:1052–1064.

Dubbink, H.J., R. Hersmus, C.S. Verma, H.A.G.M. van der Korput, C.A. Berrevoets, J. van Tol, A.C.J. Ziel-van der Made, A.O. Brinkmann, A.C.W. Pike, and J. Trapman. 2004. Distinct recognition modes of FXXLF and LXXLL motifs by the androgen receptor. *Mol. Endocrinol.* 18:2132–2150.

Farla, P., R. Hersmus, B. Geverts, P.O. Mari, A.L. Nigg, H.J. Dubbink, J. Trapman, and A.B. Houtsmuller. 2004. The androgen receptor ligand-binding domain stabilizes DNA binding in living cells. *J. Struct. Biol.* 147:50–61.

Farla, P., R. Hersmus, J. Trapman, and A.B. Houtsmuller. 2005. Antiandrogens prevent stable DNA-binding of the androgen receptor. *J. Cell Sci.* 118:4187–4198.

Georget, V., J.M. Lobaccaro, B. Terouanne, P. Mangeat, J.-C. Nicolas, and C. Sultan. 1997. Trafficking of the androgen receptor in living cells with fused green fluorescent protein-androgen receptor. *Mol. Cell. Endocrinol.* 129:17–26.

Grande, M., I. van der Kraan, L. de Jong, and R. van Driel. 1997. Nuclear distribution of transcription factors in relation to sites of transcription and RNA polymerase II. *J. Cell Sci.* 110:1781–1791.

He, B., J.A. Kemppainen, and E.M. Wilson. 2000. FXXLF and WXXLF sequences mediate the NH2-terminal interaction with the ligand binding domain of the androgen receptor. *J. Biol. Chem.* 275:22986–22994.

He, B., N.T. Bowen, J.T. Minges, and E.M. Wilson. 2001. Androgen-induced NH2- and COOH-terminal interaction inhibits p160 coactivator recruitment by activation function 2. *J. Biol. Chem.* 276:42293–42301.

He, B., J.T. Minges, L.W. Lee, and E.M. Wilson. 2002. The FXXLF motif mediates androgen receptor-specific interactions with coregulators. *J. Biol. Chem.* 277:10226–10235.

Houtsmuller, A.B., S. Rademakers, A.L. Nigg, D. Hoogstraten, J.H.J. Hoeijmakers, and W. Vermeulen. 1999. Action of DNA repair endonuclease ERCC1/XPF in living cells. *Science.* 284:958–961.

Houtsmuller, A.B., and W. Vermeulen. 2001. Macromolecular dynamics in living cell nuclei revealed by fluorescence redistribution after photobleaching. *Histochem. Cell Biol.* 115:13–21.

Hur, E., S.J. Pfaff, E.S. Payne, H. Gron, B.M. Buehrer, and R.J. Fletterick. 2004. Recognition and accommodation at the androgen receptor coactivator binding interface. *PLoS Biol.* 2:E274.

Jackson, D.A., A.B. Hassan, R.J. Errington, and P.R. Cook. 1993. Visualization of focal sites of transcription within human nuclei. *EMBO J.* 12:1059–1065.

Kang, H.-Y., S. Yeh, N. Fujimoto, and C. Chang. 1999. Cloning and characterization of human prostate coactivator ARA54, a novel protein that associates with the androgen receptor. *J. Biol. Chem.* 274:8570–8576.

Kenworthy, A.K. 2001. Imaging protein-protein interactions using fluorescence resonance energy transfer microscopy. *Methods.* 24:289–296.

Marcelli, M., D.L. Stenoien, A.T. Szafran, S. Simeoni, I.U. Agoulnik, N.L. Weigel, T. Moran, I. Mikic, J.H. Price, and M.A. Mancini. 2006. Quantifying effects of ligands on androgen receptor nuclear translocation, intranuclear dynamics, and solubility. *J. Cell. Biochem.* 98:770–788.

McNally, J.G., W.G. Müller, D. Walker, R. Wolford, and G.L. Hager. 2000. The glucocorticoid receptor: rapid exchange with regulatory sites in living cells. *Science.* 287:1262–1265.

Métivier, R., G. Reid, and F. Gannon. 2006. Transcription in four dimensions: nuclear receptor-directed initiation of gene expression. *EMBO Rep.* 7:161–167.

Michalides, R., A. Griekspoor, A. Balkenende, D. Verwoerd, L. Janssen, K. Jalink, A. Floore, A. Velds, L. van 't Veer, and J. Neefjes. 2004. Tamoxifen resistance by a conformational arrest of the estrogen receptor α PKA activation in breast cancer. *Cancer Cell.* 5:597–605.

Phair, R.D., P. Scaffidi, C. Elbi, J. Vecerova, A. Dey, K. Ozato, D.T. Brown, G. Hager, M. Bustin, and T. Misteli. 2004. Global nature of dynamic protein-chromatin interactions in vivo: three-dimensional genome scanning and dynamic interaction networks of chromatin proteins. *Mol. Cell. Biol.* 24:6393–6402.

Rayasam, G.V., C. Elbi, D.A. Walker, R. Wolford, T.M. Fletcher, D.P. Edwards, and G.L. Hager. 2005. Ligand-specific dynamics of the progesterone receptor in living cells and during chromatin remodeling in vitro. *Mol. Cell. Biol.* 25:2406–2418.

Rosenfeld, M.G., V.V. Lunyak, and C.K. Glass. 2006. Sensors and signals: a coactivator/corepressor/epigenetic code for integrating signal-dependent programs of transcriptional response. *Genes Dev.* 20:1405–1428.

Schaaf, M.J., and J.A. Cidlowski. 2003. Molecular determinants of glucocorticoid receptor mobility in living cells: the importance of ligand affinity. *Mol. Cell. Biol.* 23:1922–1934.

Schaufele, F., X. Carbonell, M. Guerbadot, S. Borngraeber, M.S. Chapman, A.A.K. Ma, J.N. Miner, and M.I. Diamond. 2005. The structural basis of androgen receptor activation: intramolecular and intermolecular amino-carboxy interactions. *Proc. Natl. Acad. Sci. USA.* 102:9802–9807.

Stenoien, D.L., K. Patel, M.G. Mancini, M. Dutertre, C.L. Smith, B.W. O'Malley, and M.A. Mancini. 2001. FRAP reveals that mobility of oestrogen receptor-alpha is ligand- and proteasome-dependent. *Nat. Cell Biol.* 3:15–23.

Sui, X., K.S. Bramlett, M.C. Jorge, D.A. Swanson, A.C. von Eschenbach, and G. Jenster. 1999. Specific androgen receptor activation by an artificial coactivator. *J. Biol. Chem.* 274:9449–9454.

Van de Wijngaart, D.J., M.E. van Royen, R. Hersmus, A.C.W. Pike, A.B. Houtsmuller, G. Jenster, J. Trapman, and H.J. Dubbink. 2006. Novel FXXFF and FXXMF motifs in androgen receptor cofactors mediate high affinity and specific interactions with the ligand-binding domain. *J. Biol. Chem.* 281:19407–19416.

Van Steensel, B., M. Brink, K. Van der Meulen, E. Van Binnendijk, D. Wansink, L. De Jong, E. De Kloet, and R. Van Driel. 1995. Localization of the glucocorticoid receptor in discrete clusters in the cell nucleus. *J. Cell Sci.* 108:3003–3011.

Wansink, D., W. Schul, I. Van der Kraan, B. Van Steensel, R. Van Driel, and L. De Jong. 1993. Fluorescent labeling of nascent RNA reveals transcription by RNA polymerase II in domains scattered throughout the nucleus. *J. Cell Biol.* 122:283–293.